HHS Public Access

Author manuscript

J Electroanal Chem (Lausanne). Author manuscript; available in PMC 2017 December 01.

Published in final edited form as:

J Electroanal Chem (Lausanne). 2016 December 1; 782: 174–181. doi:10.1016/j.jelechem.2016.10.013.

Electrochemical impedance spectroscopy study of carbohydrate-terminated alkanethiol monolayers on nanoporous gold: Implications for pore wetting

Abeera Sharma, **Jay K. Bhattarai**, **Swati S. Nigudkar**, **Salvatore G. Pistorio**, **Alexei V. Demchenko**, and **Keith J. Stine**

Department of Chemistry and Biochemistry, University of Missouri–Saint Louis, Saint Louis, MO 63121

Abstract

Electrochemical impedance spectroscopy (EIS) is used to compare the apparent electron transfer rate constant (k_{app}) for a series of alkanethiol and of carbohydrate-terminated alkanethiol self-assembled monolayers (SAMs) on both flat gold and on nanoporous gold (np-Au). Using the surface area for np-Au determined by oxide stripping, the values of k_{app} for the alkanethiol modified np-Au are initially over two orders of magnitude smaller than the values found on flat Au. This result provides evidence that the diffusing redox probe $Fe(CN)_6^{3-/4-}$ only accesses a fraction of the np-Au surface after alkanethiol modification suggesting very limited wetting of the internal pores due to the hydrophobic nature of these surfaces. In contrast, for np-Au modified by carbohydrate-terminated (mannose or galactose) alkanethiols the values of k_{app} are about 10–40 fold smaller than on flat gold, suggesting more extensive access of the diffusing redox probe within the pores and better but still incomplete wetting, a result also found for modification of np-Au with mercaptododecanoic acid. A short chain PEG thiol derivative is found to result in a comparison of k_{app} values that suggests nearly complete wetting of the internal pores for this highly hydrophilic derivative. These results are of significance for the potential applications of SAM modified np-Au in electrochemical sensors, especially for those based on carbohydrate–protein recognition, or those of np-Au modified by SAMs with polar terminal groups.

Graphical abstract

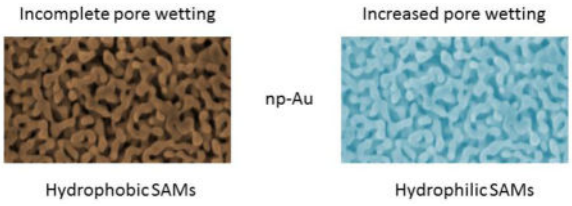

1.Introduction

Nanoporous gold (np-Au) has potential use in various technological applications because of its properties that include a high surface-to-volume ratio, a wide range of formats from thin films to large monoliths, and a tunable pore size which is easily controlled by thermal annealing treatment, acid treatment or by electrochemical methods [1–3]. Np-Au is prepared by dealloying in which any of a variety of less noble elements, such as Ag, Cu, Zn and others are removed from a precursor alloy of typically at least 20 to not more than 50 atomic percent gold [4, 5]. Np-Au has been widely investigated for used in chemical sensors, biosensors, actuators, catalysis, controlled release, supported synthesis, and as a supercapacitor [6–12].

Np-Au shows a bicontinuous structure of interconnected ligaments and gaps [2]. The ligaments present regions of positive curvature along their length with regions of negative curvature near their intersections [6]. The mean ligament width and mean ligament gap can be equivalent for prepared np-Au, but post-treatments can result in these parameters being significantly different [13]. Np-Au has been reported to retain the initial crystallographic orientation of the alloy and has been reported to be mostly Au(111) in crystal structure, but with contributions from other crystal faces [14]. Many applications of np-Au require its modification by thiol or sulfide species to form self-assembled monolayers (SAMs) inside the structure [12, 15]. The regions of positive and negative curvature could potentially affect the organization and stability of SAMs relative to what it would be on a relatively flat polycrystalline gold surface. The surface curvature may affect the orientation of alkanethiols and especially the spacing between the terminal functional groups, such as noted in a study showing that the pK_a of carboxylic acid-terminated SAMs increases with nanoparticle diameter [16, 17]. The use of SAMs with specific terminal functional groups is important, such as when these groups are activated and coupled to biomolecules for use in development of biosensors [18–20]. In a previous study using thermogravimetric analysis (TGA), we found that the coverage of an alkanethiol SAM within an np-Au monolith was close to that expected on the basis of packing geometry on flat Au [21, 22]. One recent study concerning electrochemical impedance spectroscopy (EIS) studies of alkanethiol SAMs on np-Au from octanethiol to tetradecanethiol (C8, C10, C12, and C14 chain lengths) reported that the charge transfer resistance varied gradually with chain length on np-Au but showed a steadier increase with chain length on flat gold [23]. Reductive desorption of alkanethiol SAMs on nanostructured gold surfaces of high roughness was reported to occur at more negative potentials than on close to flat polycrystalline gold, suggesting an increase in SAM stability [24].

Np-Au is a complex structure and the accessibility of solutions and of molecules in electrolyte solution to the interior surfaces is of significant interest [25]. The accessibility of unmodified np-Au to some diffusion controlled reactions such as Cu^{2+} reduction and the redox probes $Fe(CN)_6^{3-/4-}$ and $Ru(NH_3)_6^{3+/2+}$ has been evaluated using cyclic voltammetry, and it was found that the electroactive area was much less than that determined by the surface confined reaction of gold oxide monolayer formation and reduction [26]. This accessibility should also depend on the pore size and on the overall hydrophilicity or hydrophobicity of the modifying SAM. The wetting behavior and fluid penetration in np-Au

has recently been studied. It has been observed that droplets on the surface of np-Au exhibit a wetting ‘halo’ of fixed width around the circumference of a liquid drop [27]. Imbibition of electrolyte solutions into np-Au is spontaneous but can be subjected to potential control [28]. Some gold nanostructures are found to be superhydrophobic [29], and a hierarchical np-Au film has been found to be so upon modification by dodecanethiol [30].

The accessibility of electrolyte solutions to the interior surfaces of np-Au is especially important for those applications in which the high surface area of np-Au is being exploited for use as an either a high surface area electrode for use as a chemical or biological sensor, for applications involving use of np-Au for controlled release, or for applications using np-Au as a support for enzyme immobilization. These applications typically involve prior modification of the np-Au with SAMs with various terminal functional groups, and are often followed by covalent immobilization of biomolecules to the np-Au surfaces; however, accessibility is also important for cases of modification by simple physical adsorption. Accessibility of electrolyte solutions to the interior of np-Au can be viewed as significant for the efficiency of immobilization of biomolecules such as antibodies [31–33] or oligonucleotides [25, 34], sensor response [1], loading for controlled release [10, 35], and substrate access and overall activity for immobilized enzymes [36]. Carbohydrate modified np-Au has been recently explored for applications in capture and elution of lectins [21], glycoprotein modified np-Au for competitive electrochemical immunoassay, and lectin-modified np-Au for capture and subsequent elution of glycoproteins [22].

In this study, we use parameters determined from EIS data to evaluate the penetration of a solution of the diffusing redox probe $Fe(CN)_6^{3-/4-}$ into the np-Au structure upon modification with hydrophobic alkanethiols and hydrophilic mercaptododecanoic acid, carbohydrate-terminated alkanethiols, and a short chain thiolated oligooxyethylene (OEG) molecule. The OEG group is of interest not only because it is hydrophilic, but also because its derivatives are known to resist non-specific protein adsorption [37]. They are frequently used in mixed SAMs with other species presenting active functional groups [38]. EIS is a technique in which a small oscillating potential variation is applied [39], and thus differs significantly from studies using cyclic voltammetry and its large potential sweeps. The parameters extracted from EIS, such as effective electron transfer rate constant allow for comparisons that suggest that the interior surfaces of hydrophobically modified np-Au are only partially accessible to the solution of redox probe, while for the hydrophilic-terminated SAMs a much greater portion of the interior np-Au surfaces are accessible. This result is significant for efforts to develop carbohydrate-modified np-Au for applications involving carbohydrate recognition.

2. Experimental section

2.1. Materials and chemicals

Gold wire (0.2 mm diameter, 99.99%) was obtained from Electron Microscopy Sciences (Fort Washington, PA). Sodium carbonate (enzyme grade, >99%), sulfuric acid (certified ACS plus), nitric acid (trace metal grade), and hydrogen peroxide (30%), were purchased from Fisher Scientific (Pittsburg, PA). Potassium dicyanoargentate ($K[Ag(CN)_2]$) (99.96%) and potassium dicyanoaurate ($K[Au(CN)_2]$) (99.98%), ethanol (HPLC/spectrophotometric

grade), octanethiol (98.5%), decanethiol (96%), dodecanethiol (98%), tetradecanethiol (98%), 12-mercaptododecanoic acid (99%), sodium hydroxide (99.99%), sodium nitrate (99.99%), and potassium chloride (99.99%) were purchased from Sigma–Aldrich (St. Louis, MO). Milli-Q water (resistivity = 18.2 MΩ cm) was from a Simplicity® system (Millipore Corporation).

2.2. Synthesis of mannose and galactose-terminated alkanethiols

Thiolated glycosides 8-mercaptooctyl α-D-mannopyranoside (αMan-C_8-SH)), 12-mercaptooctyl α-D-mannopyranoside (αMan-C_{12}-SH)), 8-mercaptooctyl α-D-galactopyranoside (αGal-C_8-SH)), 12-mercaptooctyl α-D-galactopyranoside (αGal-C_{12}-SH)) and 8-mercapto-3,6-dioxaoctanol (HO-PEG_2-SH) were synthesized in our laboratories. The synthesis of these compounds is reported in the supplementary information file.

2.3. Preparation of nanoporous gold electrodes

Gold wires (0.2 mm diameter, 5 mm length) were thoroughly cleaned in piranha solution (4:1 H_2SO_4: H_2O_2 (30%); note: *as piranha reacts vigorously with organic solution suitable caution should be exercised*), for 10 min followed by rinsing them in Milli-Q water (resistivity = 18.2 MΩ cm). The gold wire was wrapped around the end of a copper wire (6 cm length), which was subsequently knotted and fitted through a disposable pipette tip so that the gold wire emerged from the small tip opening. The disposable pipette tip was chosen (Fisher Scientific, 1000 μL) in size to fit into the electrochemical cell assembled inside a glass vial covered by a Teflon cap with access holes for the working, reference, and counter electrode. Teflon tape was used to shield the copper wire from the solution and 5 mm of the gold wire was allowed to be exposed to the solution. An alloy of gold and silver was electrodeposited on the gold wire at −1.0 V (vs. Ag/AgCl/KCl saturated) for 10 min (due to the shell like morphology of np-Au achieved at this deposition voltage, and the time was chosen to generate a larger surface area after dealloying) in the electrochemical cell. The electrodeposition solution consisted of 6.3 mL of 0.05 M $K[Ag(CN)_2]$ and 2.7 mL of 0.05 M $K[Au(CN)_2]$ (dissolved in 0.25 M sodium carbonate) to give a total composition of 70% Ag and 30% Au in the 9.0 mL solution volume. Electrodeposition was carried out with gold wire as a working electrode, platinum wire as a counter electrode, and Ag/AgCl, KCl (saturated) as a reference electrode using a PARSTAT 2273 potentiostat and the PowerSuite software. The alloy deposited on the gold wire was then dealloyed in concentrated nitric acid for 24 h. After dealloying, the nanoporous gold covered gold electrode (referred to as np-Au electrode) was rinsed copiously with Milli-Q water for a minimum of 20 min and then kept in ethanol for 30 min to remove any trace nitric acid trapped in the pores as well to reduce any gold oxide which might have been formed on the surface [40, 41].

2.4. Determination of the surface area of the nanoporous gold electrodes

The np-Au electrodes were subject to a cyclic potential sweep between 0.5 V and 1.6 V at 0.100 Vs^{-1} in 0.5 M H_2SO_4. The charge passed under the oxide reduction peak was used to estimate the gold surface area using the conversion factor of 450 μC cm^{-2} [42].

2.5. Self-assembled monolayer preparation

The thoroughly rinsed electrodes were immersed in 1 mM ethanolic solutions of the alkanethiols or other thiolated species overnight and then upon removal were rinsed with ethanol and with Milli-Q water.

2.6. Contact angle measurement

The hydrophilic or hydrophobic nature of the SAMs prepared on the flat gold surface was characterized by measuring water contact angle. The flat gold surface was prepared by template stripping of sputtered gold from a silicon wafer. The details of this method were previously reported by our group [20]. The water contact angle was determined using a simple home-made setup (Fig. S1 in the supplementary information file) and ImageJ software with contact angle plugins, similar to the work discussed by Lamour and coworkers [43]. The mean and the standard deviation of contact angle were obtained from an average of three freshly prepared droplets.

2.7. Electrochemical impedance spectroscopy

EIS was performed in a three-electrode cell of 3 mL solution of 10 mM phosphate buffered saline of pH 7.4 containing 5 mM $K_3[Fe(CN)_6]$ and 5 mM $K_4[Fe(CN)_6]$ at the formal potential of the redox probe (0.23 V vs. Ag/AgCl/KCl saturated), which was determined by cyclic voltammetry. The EIS was performed at frequencies from 10^5 Hz to 100 mHz and at 12 points per decade. The instrument used for EIS measurement was the PARSTAT 2273 potentiostat/galvanostat/FRA using the PowerSine software to view the Nyquist plots. Data analysis was carried out using ZSimpwin 3.21 software (Princeton Applied Research, Oak Ridge, TN), and an equivalent circuit model wherein the double-layer capacitor was replaced by a constant phase element (Q) in order to account for the roughness of np-Au.

2.8. Scanning electron microscopy

Surface morphology and composition of np-Au were characterized using scanning electron microscopy (JEOL JSM-6320F field emission SEM) and energy-dispersive X-ray spectroscopy (EDX), respectively. The accelerating voltage used for our system was 5 kV and the working distance was 8 mm.

3. Results and discussion

SEM images of np-Au covered Au wires used here are shown in Fig. 1, which clearly show the interconnected structure of ligaments and gaps constituting pores that is characteristic of np-Au. The thickness of the np-Au coating on the Au wires is ~ 8 μm and is shell-like but with some microscopic crack-like features likely due to volume shrinkage during dealloying [44]. From the oxide stripping experiment (see Fig. 2), the surface area of the np-Au electrodes was estimated to be 12.8 ± 0.5 cm^2 (n = 3) as compared to the bare gold wire for which the geometric area is 0.032 cm^2 and the electrochemical surface area using the oxide stripping method is 0.036 ± 0.003 cm^2 (n = 5) indicating some surface roughness for the bare gold wire.

Nyquist plots of bare gold wire (GW) and np-Au are shown in Fig. 3a. The Nyquist plot of GW consists of a distinct semicircle, representing charge transfer resistance and a linear Warburg impedance, representing diffusion based impedance. The Nyquist plot of np-Au, however, does not show a distinct semicircle, thus representing the low impedance of the high surface area np-Au electrode. This ease of transfer of charges or electrons to and from the electrode surface minimizes the charge transfer resistance in the high frequency region. In the present study, the circuit model shown (Fig. 3b) is used for fitting both flat Au and np-Au electrodes in order to provide a basis for comparison of trends in fit parameters and the effect of SAM modification. Other more elaborate circuit models have been proposed for porous electrodes, such as the transmission line model of de Levie [45]. The de Levie model has been applied to np-Au wires in different electrolyte solutions and modification with 6-mercapto-1-hexanol was found to decrease the capacitance by about 10-fold [46]. Electrochemical techniques are well-suited for the characterization of the microscopic properties of the interface and for the characterization of the extent of defects in SAMs [47, 48]. The integrity and packing of the SAM on the substrate surface affects the electrochemical properties at the interface which are reflected in the double layer capacitance and the charge transfer resistance [49]. The extent of defects in the SAM is related to the ability of the SAM to hinder electron transfer across the interface. It has commonly been reported for alkanethiol SAMs on polycrystalline gold that an increase in chain length increases the charge transfer resistance (R_{ct}) [50]. It is of interest to determine how R_{ct} varies with chain length on np-Au versus on a flat gold surface. Nyquist plots of the SAMs of a series of alkanethiols on Au wire and also on np-Au are shown in Fig. 3c and 3d, respectively.We found that on both the np-Au and the gold wire surfaces an increase in R_{ct} with increasing chain length was observed. A recent EIS study of alkanethiol SAMs on np-Au from octanethiol to tetradecanethiol (C8, C10, C12, and C14 chain lengths) reported that R_{ct} varied gradually with chain length on np-Au but showed a steadier increase with chain length on flat gold [23]. In this reported study, the EIS measurements were conducted in 0.1 M H_2SO_4 using $Fe(CN)_6^{3-}$ as the redox probe, compared to measurements here conducted in 10 mM PBS at pH 7.4 containing 5 mM $K_3[Fe(CN)_6]$ and 5 mM $K_4[Fe(CN)_6]$ redox probe.

Charge transfer resistance is related to the electron transfer rate across the interface. The standard procedure involves fitting impedance data to an equivalent circuit model that represents the physical interface, in order to obtain R_{ct} from which the apparent electron transfer rate constant k_{app} can be calculated [51]. The apparent electron transfer rate constant for SAM modified electrodes has been calculated and used for the estimation of the extent of defects in the SAM [52–54]. The apparent electron transfer rate constant across the interface can be obtained from R_{ct} through the relation $k_{app} = RT/(n^2F^2AR_{ct}C)$ [55] where R is the gas constant, T is temperature in Kelvin (293 K in these experiments), n is the number of moles of electrons transferred in the redox reaction (n = 1 for $Fe(CN)_6^{3-/4-}$), F is the Faraday constant, $R_{ct}$is the charge transfer resistance in Ω, A is the area of the electrode, and C is the concentration of the redox couple (in mol cm^{-3}). In this expression, the fitted value of R_{ct} in Ω is multiplied by the electrode area to obtain an interfacial resistivity and thus knowledge of the accurate active electrode area is necessary. Electron transfer across the interface takes place through three major processes including non-adiabatic electron

tunneling through the SAM, electron transfer across pinhole defects where the electron transfer process is similar to that on the bare metallic surface and electron transfer across the collapsed SAM sites [56]. The apparent electron transfer rate constant is a measure of the electron transfer kinetics across the interface and increases with an increase in the number of defects in the SAM caused by several factors including defects in the underlying substrate, kinks edges, grain boundaries, or trapped solvent [57, 58].

The values of the electron transfer resistance and the apparent electron transfer rate for the alkanethiol SAMs are shown in table I (error bars are for three independently prepared modified electrodes). The values of R_{ct} are multiplied either by the geometric surface area for the SAMs on Au wire, or by the area determined by oxide stripping for the np-Au electrodes. The values of k_{app} for the alkanethiol SAMs on np-Au as calculated are lower than those found on flat Au by factors of 150 for octanethiol and by factors of 367, 382, and 408 for decanethiol, dodecanethiol and tetradecanethiol, respectively. It is noteworthy that the smaller difference is for the shorter octanethiol which may present the less ordered and somewhat less hydrophobic surface. Fig. 4a shows the variation of R_{ct} (units of kΩ) as determined by the fits to the Nyquist plots versus chain length on np-Au (circles) and on Au wire electrodes (squares) and the variation of log(k_{app}) as calculated using R_{ct} in units of Ω cm^2 with chain length on np-Au and on flat gold is shown in Fig. 4b. SAMs on the surface of np-Au are not expected to yield the same electron transfer rates as seen on flat gold; however, it is not reasonable to attribute these much smaller values of k_{app} to greater order in the SAMs on np-Au. The electron transfer rates are shown to nearly approach a limiting value with tetradecanethiol having the lowest k_{app} value, as expected for the SAMs of longest chain length. If the electrolyte solution does not wet the hydrophobic interior surface of the alkanethiol-modified np-Au, then electron transfer rate constants calculated using the estimated area of the np-Au surface of 12.8 cm^2 will be artificially low by a significant factor. The calculated values on np-Au using the full np-Au surface area are lower than those on gold wire by factors close to 400 for the three longer alkanethiols, which is fairly consistent with the ratio 12.8 cm^2/0.032 cm^2 = 400 for the amplification of total surface area between gold wire and np-Au covered Au wire. This observation suggests that the internal surfaces of np-Au when it has been made sufficiently hydrophobic by surface modification with a longer alkanethiol are not penetrated by the electrolyte solution.

Nyquist plots for the carbohydrate-terminated SAMs on np-Au are shown in Fig. 5, and for the short-chain OEG derivative HO-PEG_2-SH (TEG), and for mercaptododecanoic acid (MDDA) in Fig. 6. The semicircles in the Nyquist plots for these hydrophilic SAMs do not close at low frequencies as fully as do those for the alkanethiol SAMs and hence the R_{ct} values from the fits are determined by the existing curvature. The values for the R_{ct} and the k_{app} of these SAMs are also shown in Table II. For the case of the HO-PEG_2-SH derivative, the value of k_{app} calculated using the estimated surface area of np-Au differs from the value found on Au wire only by a factor of 1.34. This result suggests that the electrolyte solution wets the internal surfaces of np-Au when it is modified by this small highly hydrophilic species. For the case of mercaptododecanoic acid, the difference in k_{app} calculated on Au wire versus on np-Au is a factor of 41, which is significant but less of a difference than seen for the alkanethiol SAMs summarized in table I or for dodecanethiol. This result suggests partial wetting/penetration of the np-Au interior after modification by mercaptododecanoic

acid, aided by the polar terminal carboxyl group. For the mannose-terminated SAMs, we see differences in k_{app} by factors of 15 (αMan-C_8-SH) and 9 (αMan-C_{12}-SH), and for the galactose-terminated SAMs, we see differences in k_{app} by factors of 11 (αGal-C_8-SH) and 40 (αGal-C_{12}-SH). These results also suggest better wetting/penetration of the np-Au interior when modified by the hydrophilic carbohydrate-presenting SAMs; however, the wetting/penetration is expected to be still partial.

The contact angles of water droplets on the different SAMs prepared on flat gold surfaces were determined using a simple home-built setup and ImageJ software, as shown in Fig. S1 and in Fig. S2 in the supplementary information file. Estimation of the water contact angle helps to determine the wettability of the surface. If the contact angle is larger than 90°, the surface is hydrophobic, and if below 90°, it is hydrophilic [59]. The bare flat gold surface is slightly hydrophilic in nature, and the water contact angle was found to be 71 ± 4° very closely matching the literature value ~66–70° [60, 61], even though the flat gold was prepared using different techniques. Immobilization of hydrophobic C_{12}-SH on the gold surface increases the contact angle from 71 ± 4° to 104 ± 2°, decreasing the wettability and this value is in accordance with the previously reported values 103 ± 3° [62] and 110° [63]. These very closely matching contact angles of bare flat gold and SAMs of C_{12}-SH with the literature values helps us verify the sensitivity of our simple home-made setup. Similarly, the contact angle for water droplets on mannose and galactose-terminated alkanethiol SAMs were determined. We have found that both carbohydrate SAMs are hydrophilic due to the presence of a large number of hydroxyl groups. Interestingly, the galactose-terminated surface (contact angle = 17 ± 2°) was found to be more hydrophilic compared to the mannose-terminated surface (contact angle = 31 ± 5°). Dietrich and coworkers determined the contact angle of dimannoside SAM on gold surface getting a value close to 36 ± 2° [64]. Dimannoside, containing even more hydroxyl groups, should be very hydrophilic and nearly total wetting was expected. The authors explained that the slightly larger contact angle seen might be due to the hydrophobic aliphatic linker chain. For galactose SAMs with a slightly different linker than ours, total wetting has been observed [65]. The carboxyl-terminated alkanethiol shows a contact angle of 39 ± 3° which is slightly lower than the reported value 50 ± 2° [62]. Finally, the contact angle of HO-PEG_2-SH SAMs has been determined to be 64± 3°. The contact angle of a SAM closely related in structure to HO-PEG_2-SH for comparison is not available; however, when larger alkane chains are attached to the HO-PEG_2-SH, the contact angle was found to be small, close to 32–36° [66]. These angles are lower than the contact angle of our HO-PEG_2-SH SAMs. The larger contact angle of HO-PEG_2-SH may be due to its short length and greater exposure of Au surface to water. Despite the higher contact angle, EIS indicates that HO-PEG_2-SH surfaces are likely fully wetted. Contact angle is only one method and further work with other techniques may be needed to understand these trends that could be related to the SAM structure on the np-Au surfaces. For the other SAMs, the measured values of the contact angles are found to be in general agreement with the results obtained by the EIS.

The effect of the immersion time of electrode in a probe solution for wetting was studied by choosing different time periods of 1, 10, 30, 60, and 120 min prior to EIS measurement. It was found that np-Au electrodes modified by hydrophilic SAMs did not show any significant change in R_{ct} value with increasing immersion time. However, np-Au electrodes

modified by hydrophobic SAMs exhibited a significant decrease in the R_{ct} value with the increase in immersion time. From this experiment, it can be concluded that hydrophilic SAMs wet the porous electrode to the extent that they will within a minute and then exhibit little subsequent change. However, for the hydrophobic alkanethiol SAMs on np-Au, the electrolyte solution can penetrate slowing inside the porous structures decreasing the charge transfer resistance over time. The results of the experiment are shown in the supplementary information, Fig. S3, where it is seen that for the dodecanethiol SAMs, the value of R_{ct} decreases by about 95% over a 2 h period and appears to be leveling off. This decrease of about an order of magnitude still represents only partial wetting and may be driven by bare spots in the SAM as its structure may be compromised by the complexity of the curved np-Au surfaces. In any case, it indicates that caution must be applied to electrochemical measurements conducted on SAM modified np-Au electrodes and their wetting behavior.

4. Conclusions

The electrochemical behavior of SAMs in np-Au is complex and varies with the polarity of the SAM. For more hydrophilic and polar SAM modified np-Au, there is greater penetration of the electrolyte solution and hence of the redox probe into the interior channels of the material. Thus, electrochemical sensors that are based on more hydrophilic SAM/solution interfaces are likely to generate greater currents, both in terms of Faradaic and non-Faradaic contributions. The results presented here suggest that SAM/solution interfaces of high hydrophilicity are likely to yield increased access for analytes and enzyme substrates, and increased loadings in bioconjugation reactions conducted under static solution conditions. The conclusion is reached based on comparing determined values of k_{app} using the geometric surface area with those determined using the surface area from gold oxide stripping. The discrepancy in magnitude of k_{app} becomes less when the SAMs are more polar such as 12-mercaptododecanoic acid, HO-PEG_2-SH or for carbohydrate-terminated SAMs that are of significance in the study of protein (lectins, in particular)–carbohydrate interaction using electrochemical methods.

Supplementary Material

Refer to Web version on PubMed Central for supplementary material.

Acknowledgments

This work was supported by University of Missouri–St. Louis and by the NIGMS awards R01-GM090254 and GM111835.

References

1. Collinson MM. Nanoporous gold electrodes and their applications in analytical chemistry. ISRN Anal Chem. 2013; 2013
2. Sharma A, Bhattarai JK, Alla AJ, Demchenko AV, Stine KJ. Electrochemical annealing of nanoporous gold by application of cyclic potential sweeps. Nanotechnology. 2015; 26:085602. [PubMed: 25649027]
3. Dorofeeva TS, Seker E. Electrically tunable pore morphology in nanoporous gold thin films. Nano Res. 2015; 8:2188–2198.

4. Seker E, Reed ML, Begley MR. Nanoporous gold: fabrication, characterization, and applications. Materials. 2009; 2:2188–2215.
5. Jia F, Yu C, Ai Z, Zhang L. Fabrication of nanoporous gold film electrodes with ultrahigh surface area and electrochemical activity. Chem Mater. 2007; 19:3648–3653.
6. Fujita T, Guan P, McKenna K, Lang X, Hirata A, Zhang L, Tokunaga T, Arai S, Yamamoto Y, Tanaka N, Ishikawa Y, Asao N, Yamamoto Y, Erlebacher J, Chen M. Atomic origins of the high catalytic activity of nanoporous gold. Nat Mater. 2012; 11:775–780. [PubMed: 22886067]
7. Wittstock A, Wichmann A, Bäumer M. Nanoporous gold as a platform for a building block catalyst. ACS Catal. 2012; 2:2199–2215.
8. Qiu HJ, Zhou GP, Ji GL, Zhang Y, Huang XR, Ding Y. A novel nanoporous gold modified electrode for the selective determination of dopamine in the presence of ascorbic acid. Colloids Surf B: Biointerfaces. 2009; 69:105–108. [PubMed: 19108998]
9. Pandey B, Bhattarai JK, Pornsuriyasak P, Fujikawa K, Catania R, Demchenko AV, Stine KJ. Square-wave voltammetry assays for glycoproteins on nanoporous gold. J Electroanal Chem. 2014; 717–718:47–60.
10. Kurtulus O, Daggumati P, Seker E. Molecular release from patterned nanoporous gold thin films. Nanoscale. 2014; 6:7062–7071. [PubMed: 24842586]
11. Hou Y, Chen L, Hirata A, Fujita T, Chen M. Non-aqueous nanoporous gold based supercapacitors with high specific energy. Scr Mater. 2016; 116:76–81.
12. Shulga OV, Zhou D, Demchenko AV, Stine KJ. Detection of free prostate specific antigen (fPSA) on a nanoporous gold platform. Analyst. 2008; 133:319–322. [PubMed: 18299744]
13. Tan YH, Davis JA, Fujikawa K, Ganesh NV, Demchenko AV, Stine KJ. Surface area and pore size characteristics of nanoporous gold subjected to thermal, mechanical, or surface modification studied using gas adsorption isotherms, cyclic voltammetry, thermogravimetric analysis, and scanning electron microscopy. J Mater Chem. 2012; 22:6733–6745. [PubMed: 22822294]
14. Stowers K, Madix R, Friend C. From model studies on Au (111) to working conditions with unsupported nanoporous gold catalysts: Oxygen-assisted coupling reactions. J Catal. 2013; 308:131–141.
15. Chen L, Fujita T, Chen M. Biofunctionalized nanoporous gold for electrochemical biosensors. Electrochim Acta. 2012; 67:1–5.
16. Arnold R, Azzam W, Terfort A, Wöll C. Preparation, modification and crystallinity of aliphatic and aromatic carboxylic acid terminated self-assembled monolayers. Langmuir. 2002; 18:3980–3992.
17. Zhang H, Zhou Z, Yang B, Gao M. The influence of carboxyl groups on the photoluminescence of mercaptocarboxylic acid-stabilized CdTe nanoparticles. J Phys Chem B. 2003; 107:8–13.
18. Tan YH, Pandey B, Sharma A, Bhattarai J, Stine KJ. Bioconjugation reactions for covalent coupling of proteins to gold surfaces. Global J Biochem. 2012; 3:6.
19. Sonawane MD, Nimse SB. Surface modification chemistries of materials used in diagnostic platforms with biomolecules. J Chem. 2016; 2016:19.
20. Bhattarai JK, Sharma A, Fujikawa K, Demchenko AV, Stine KJ. Electrochemical synthesis of nanostructured gold film for the study of carbohydrate–lectin interactions using localized surface plasmon resonance spectroscopy. Carbohydr Res. 2015; 405:55–65. [PubMed: 25442712]
21. Tan YH, Fujikawa K, Pornsuriyasak P, Alla AJ, Ganesh NV, Demchenko AV, Stine KJ. Lectin–carbohydrate interactions on nanoporous gold monoliths. New J Chem. 2013; 37:2150–2165.
22. Alla AJ, d'Andrea FB, Bhattarai JK, Cooper JA, Tan YH, Demchenko AV, Stine KJ. Selective capture of glycoproteins using lectin-modified nanoporous gold monolith. J Chromatogr A. 2015; 1423:19–30. [PubMed: 26554297]
23. Chu Y, Seo B, Kim J. Electrochemical properties of alkanethiol monolayers adsorbed on nanoporous au surfaces. Bull Korean Chem Soc. 2010; 31:3407–3410.
24. Cortés E, Rubert AA, Benitez G, Carro P, Vela ME, Salvarezza RC. Enhanced stability of thiolate self-assembled monolayers (SAMs) on nanostructured gold substrates. Langmuir. 2009; 25:5661–5666. [PubMed: 19348488]
25. Daggumati P, Matharu Z, Seker E. Effect of nanoporous gold thin film morphology on electrochemical DNA sensing. Anal Chem. 2015; 87:8149–8156. [PubMed: 25892217]

26. Scanlon MD, Salaj-Kosla U, Belochapkine S, MacAodha D, Leech D, Ding Y, Magner E. Characterization of nanoporous gold electrodes for bioelectrochemical applications. Langmuir. 2011; 28:2251–2261. [PubMed: 22004670]
27. Seker E, Tauer T, Zhu J, Begley M, Bart-Smith H, Zangari G, Kelly RG, Utz M, Reed ML. Wetting phenomenon in nanoporous gold films. ECS Trans. 2007; 6:83–89.
28. Xue Y, Markmann J, Duan H, Weissmüller J, Huber P. Switchable imbibition in nanoporous gold. Nat commun. 2014; 5
29. Zhang H, Xu J-J, Chen H-Y. Shape-controlled gold nanoarchitectures: synthesis, superhydrophobicity, and electrocatalytic properties. J Phys Chem C. 2008; 112:13886–13892.
30. Huang W, Wang M, Zheng J, Li Z. Facile fabrication of multifunctional three-dimensional hierarchical porous gold films via surface rebuilding. J Phys Chem C. 2009; 113:1800–1805.
31. Pandey B, Demchenko AV, Stine KJ. Nanoporous gold as a solid support for protein immobilization and development of an electrochemical immunoassay for prostate specific antigen and carcinoembryonic antigen. Microchim Acta. 2012; 179:71–81.
32. Wei Q, Zhao Y, Xu C, Wu D, Cai Y, He J, Li H, Du B, Yang M. Nanoporous gold film based immunosensor for label-free detection of cancer biomarker. Biosens Bioelectron. 2011; 26:3714–3718. [PubMed: 21392961]
33. Ding C, Li H, Hu K, Lin J-M. Electrochemical immunoassay of hepatitis B surface antigen by the amplification of gold nanoparticles based on the nanoporous gold electrode. Talanta. 2010; 80:1385–1391. [PubMed: 20006103]
34. Daggumati P, Appelt S, Matharu Z, Marco ML, Seker E. Sequence-specific electrical purification of nucleic acids with nanoporous gold electrodes. J Am Chem Soc. 2016; 138:7711–7717. [PubMed: 27244455]
35. Polat O, Seker E. Halide-gated molecular release from nanoporous gold thin films. J Phys Chem C. 2015; 119:24812–24818.
36. Stine, KJ., Jefferson, K., Shulga, OV. Nanoporous gold for enzyme immobilization. In: Minteer, DS., editor. Enzyme Stabilization and Immobilization: Methods and Protocols. Humana Press; Totowa, NJ: 2011. p. 67-83.
37. Bhattarai, JK., Tan, YH., Pandey, B., Fujikawa, K., Demchenko, AV., Stine, KJ. Electrochemical impedance spectroscopy study of Concanavalin A binding to self-assembled monolayers of mannosides on gold wire electrodes. J Electroanal Chem. http://dx.doi.org/10.1016/j.jelechem.2016.09.045
38. Houseman BT, Gawalt ES, Mrksich M. Maleimide-functionalized self-assembled monolayers for the preparation of peptide and carbohydrate biochips. Langmuir. 2003; 19:1522–1531.
39. Chang B-Y, Park S-M. Electrochemical impedance spectroscopy. Annu Rev Anal Chem. 2010; 3:207–229.
40. He X, Antonelli D. Recent advances in synthesis and applications of transition metal containing mesoporous molecular sieves. Angew Chem Int Ed. 2002; 41:214–229.
41. Ron H, Rubinstein I. Self-assembled monolayers on oxidized metals. 3. Alkylthiol and dialkyl disulfide assembly on gold under electrochemical conditions. J Am Chem Soc. 1998; 120:13444–13452.
42. Evans U, Colavita PE, Doescher MS, Schiza M, Myrick ML. Construction and characterization of a nanowell electrode array. Nano Lett. 2002; 2:641–645.
43. Lamour G, Hamraoui A, Buvailo A, Xing Y, Keuleyan S, Prakash V, Eftekhari-Bafrooei A, Borguet E. Contact angle measurements using a simplified experimental setup. J Chem Educ. 2010; 87:1403–1407.
44. Seker E, Reed ML, Begley MR. A thermal treatment approach to reduce microscale void formation in blanket nanoporous gold films. Scr Mater. 2009; 60:435–438.
45. Chae W-S, Gough DV, Ham S-K, Robinson DB, Braun PV. Effect of ordered intermediate porosity on ion transport in hierarchically nanoporous electrodes. ACS appl mater interfaces. 2012; 4:3973–3979. [PubMed: 22799397]
46. Robinson, DB., Wu, C-AM., Jacobs, BW., Ong, MD., Tran, KL., Langham, ME., Ha, CM., Gough, DV., Braun, PV., Chae, W-S. Optimized nanoporous materials. Sandia National Laboratory; 2009.

47. Leopold MC, Doan TT, Mullaney MJ, Loftus AF, Kidd CM. Electrochemical characterization of self-assembled monolayers on gold substrates derived from thermal decomposition of monolayer-protected cluster films. J Appl Electrochem. 2015; 45:1069–1084.
48. Fioravanti G, Lugli F, Gentili D, Mucciante V, Leonardi F, Pasquali L, Liscio A, Murgia M, Zerbetto F, Cavallini M. Electrochemical fabrication of surface chemical gradients in thiol self-assembled monolayers with tailored work-functions. Langmuir. 2014; 30:11591–11598. [PubMed: 25222857]
49. Eckermann AL, Feld DJ, Shaw JA, Meade TJ. Electrochemistry of redox-active self-assembled monolayers. Coord Chem Rev. 2010; 254:1769–1802. [PubMed: 20563297]
50. Ding S-J, Chang B-W, Wu C-C, Lai M-F, Chang H-C. Impedance spectral studies of self-assembly of alkanethiols with different chain lengths using different immobilization strategies on Au electrodes. Anal Chim Acta. 2005; 554:43–51.
51. Ganesh V, Pal SK, Kumar S, Lakshminarayanan V. Self-assembled monolayers (SAMs) of alkoxycyanobiphenyl thiols on gold—A study of electron transfer reaction using cyclic voltammetry and electrochemical impedance spectroscopy. J Colloid Interface Sci. 2006; 296:295–303.
52. Diao P, Guo M, Jiang D, Jia Z, Cui X, Gu D, Tong R, Zhong B. Fractional coverage of defects in self-assembled thiol monolayers on gold. J Electroanal Chem. 2000; 480:59–63.
53. Sabatani E, Rubinstein I. Organized self-assembling monolayers on electrodes. 2. Monolayer-based ultramicroelectrodes for the study of very rapid electrode kinetics. J Phys Chem. 1987; 91:6663–6669.
54. Aguiar FA, Campos R, Wang C, Jitchati R, Batsanov AS, Bryce MR, Kataky R. Comparative electrochemical and impedance studies of self-assembled rigid-rod molecular wires and alkanethiols on gold substrates. Phys Chem Chem Phys. 2010; 12:14804–14811. [PubMed: 20890500]
55. Nkosi D, Pillay J, Ozoemena KI, Nouneh K, Oyama M. Heterogeneous electron transfer kinetics and electrocatalytic behaviour of mixed self-assembled ferrocenes and SWCNT layers. Phys Chem Chem Phys. 2010; 12:604–613. [PubMed: 20066346]
56. Diao P, Guo M, Tong R. Characterization of defects in the formation process of self-assembled thiol monolayers by electrochemical impedance spectroscopy. J Electroanal Chem. 2001; 495:98–105.
57. Finklea HO, Avery S, Lynch M, Furtsch T. Blocking oriented monolayers of alkyl mercaptans on gold electrodes. Langmuir. 1987; 3:409–413.
58. Kiani A, Alpuche-Aviles MA, Eggers PK, Jones M, Gooding JJ, Paddon-Row MN, Bard AJ. Scanning electrochemical microscopy. 59. Effect of defects and structure on electron transfer through self-assembled monolayers. Langmuir. 2008; 24:2841–2849. [PubMed: 18237208]
59. Yuan, Y., Lee, TR. Surface science techniques. Springer; 2013. Contact angle and wetting properties; p. 3-34.
60. Abdelsalam ME, Bartlett PN, Kelf T, Baumberg J. Wetting of regularly structured gold surfaces. Langmuir. 2005; 21:1753–1757. [PubMed: 15723469]
61. Grell TA, Alabanza AM, Gaskell K, Aslan K. Microwave-accelerated surface modification of plasmonic gold thin films with self-assembled monolayers of alkanethiols. Langmuir. 2013; 29:13209–13216. [PubMed: 24083414]
62. Li J, Guan T, Hao C, Li L, Zhang Y. Effects of self-assembled monolayers with different chemical groups on ovarian cancer cell line behavior in vitro. J Chem. 2015; 2015:10.
63. Shi F, Wang Z, Zhang X. Combining a layer-by-layer assembling technique with electrochemical deposition of gold aggregates to mimic the legs of water striders. Adv Mater. 2005; 17:1005–1009.
64. Dietrich PM, Horlacher T, Girard-Lauriault PL, Gross T, Lippitz A, Min H, Wirth T, Castelli R, Seeberger PH, Unger WE. Adlayers of dimannoside thiols on gold: surface chemical analysis. Langmuir. 2011; 27:4808–4815. [PubMed: 21417247]
65. Hederos M, Konradsson P, Liedberg B. Synthesis and self-assembly of galactose-terminated alkanethiols and their ability to resist proteins. Langmuir. 2005; 21:2971–2980. [PubMed: 15779973]

66. Schwendel D, Hayashi T, Dahint R, Pertsin A, Grunze M, Steitz R, Schreiber F. Interaction of water with self-assembled monolayers: neutron reflectivity measurements of the water density in the interface region. Langmuir. 2003; 19:2284–2293.

Highlights

- Impedance spectroscopy applied to self-assembled monolayers (SAMs) on gold and on nanoporous gold (np-Au)
- Comparison of a series of alkanethiols as SAMs on both surfaces
- Comparison of carbohydrate terminated alkanethiols as SAMs on both surfaces
- Results for electron transfer rate constants suggest limited wetting of alkanethiol modified np-Au
- Results suggest partial wetting with carbohydrate derivatives and full wetting with an oxyethylene derivative

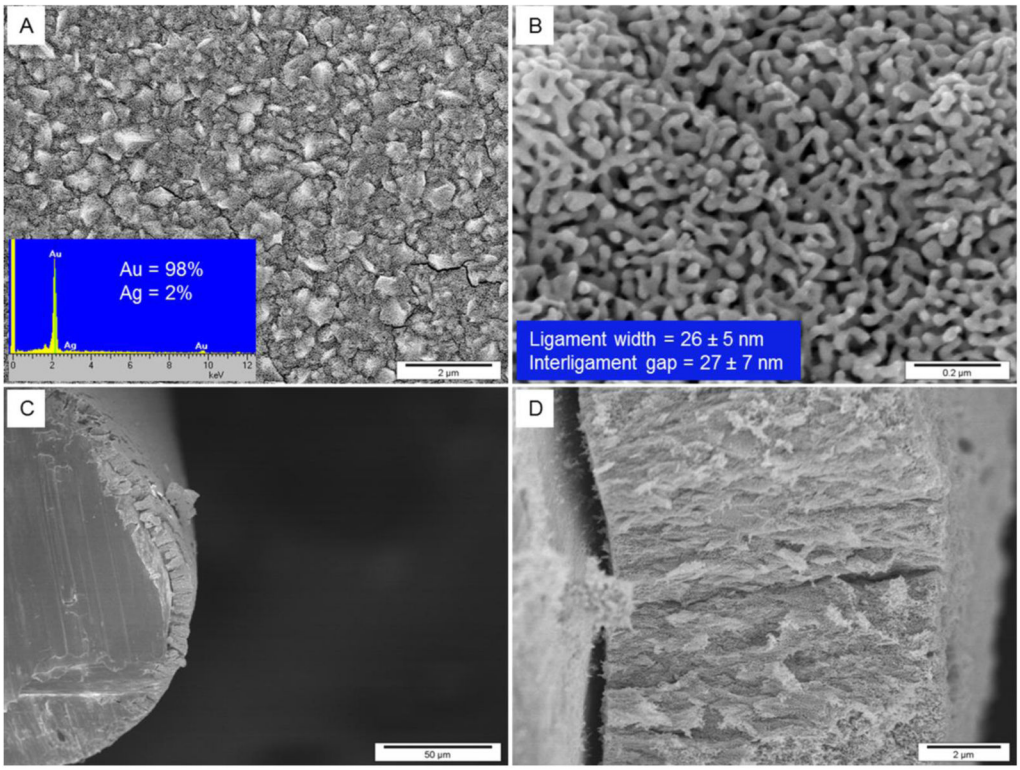

Fig. 1.

SEM images of np-Au obtained by 24 h selective dissolution of Ag in concentrated HNO_3 from Au–Ag alloy. The alloy was prepared by providing −1.0 V (vs. Ag/AgCl, KCl saturated) for 10 min on gold wire. A and B are top views with increasing magnification showing cracks formation and pore morphology, respectively. Inset in A represents the EDX spectra showing Au and Ag composition and inset in B gives the ligament width and interligament gap. Panels C and D are cross-sectional views with increasing magnification showing thickness of np-Au of around 8 μM and inter-connected ligaments and gaps throughout the structure.

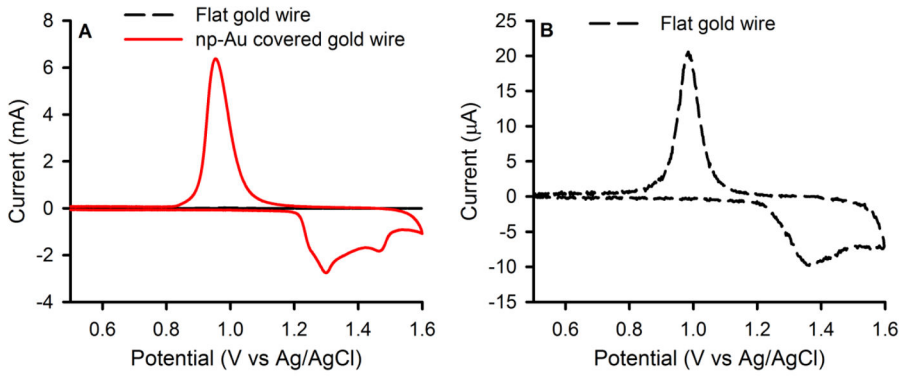

Fig. 2.

(a) Comparison of cyclic voltammograms (CV) of flat gold wire and np-Au covered gold wire, and (b) CV of flat gold wire on an expanded scale. CVs were used for the determination of the surface area of flat gold and np-Au electrodes and were obtained in 0.5 M H_2SO_4 at a scan rate of 100 mV s^{-1} (vs Ag/AgCl/KCl saturated).

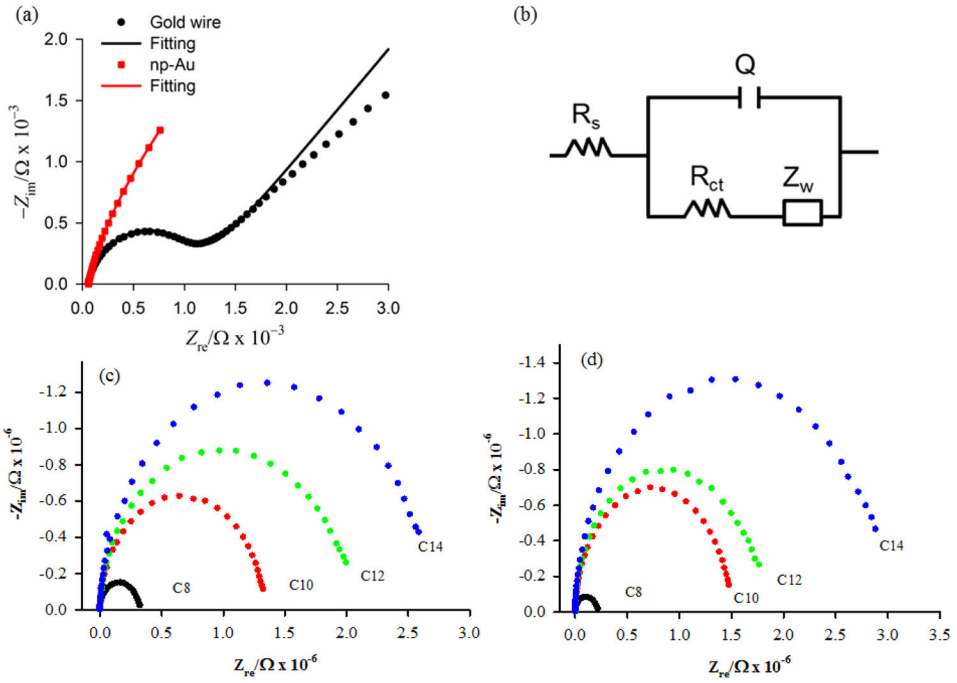

Fig. 3.

Nyquist plots of (a) a bare gold wire and np-Au electrode and (c-d) after SAMs formation from a series of alkanethiols (octanethiol, decanethiol, dodecanethiol, and tetradecanethiol) on Au wire and np-Au electrode, respectively. For each case, plots are obtained for three independently prepared electrodes. (b) Circuit model used for analysis of the EIS data.

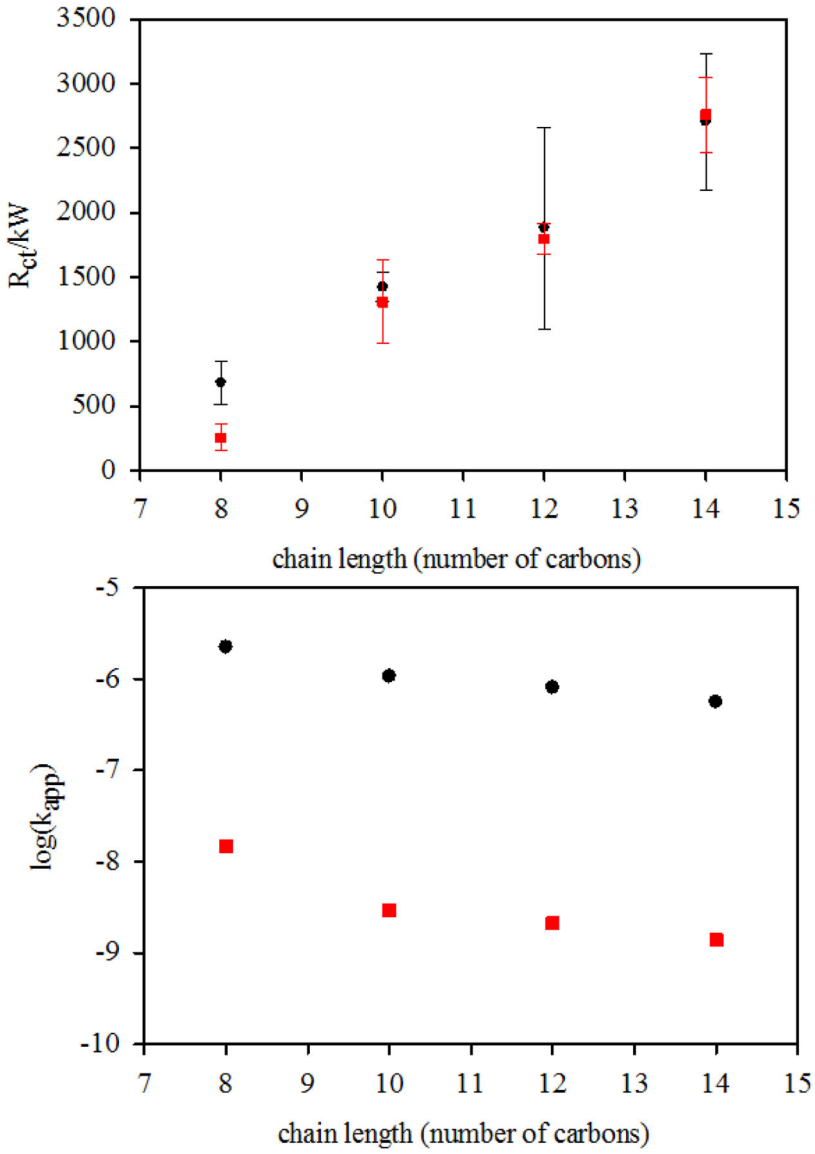

Fig. 4.

(a) Plot of R_{ct} versus alkanethiol chain length on np-Au (squares) and Au wire electrodes (circles), (b) plot of log(k_{app}) vs chain length for alkanethiols as calculated on np-Au using the surface area of 12.8 cm^2 (squares) from oxide stripping and on flat gold wire electrodes (circles) using the geometric area of 0.032 cm^2.

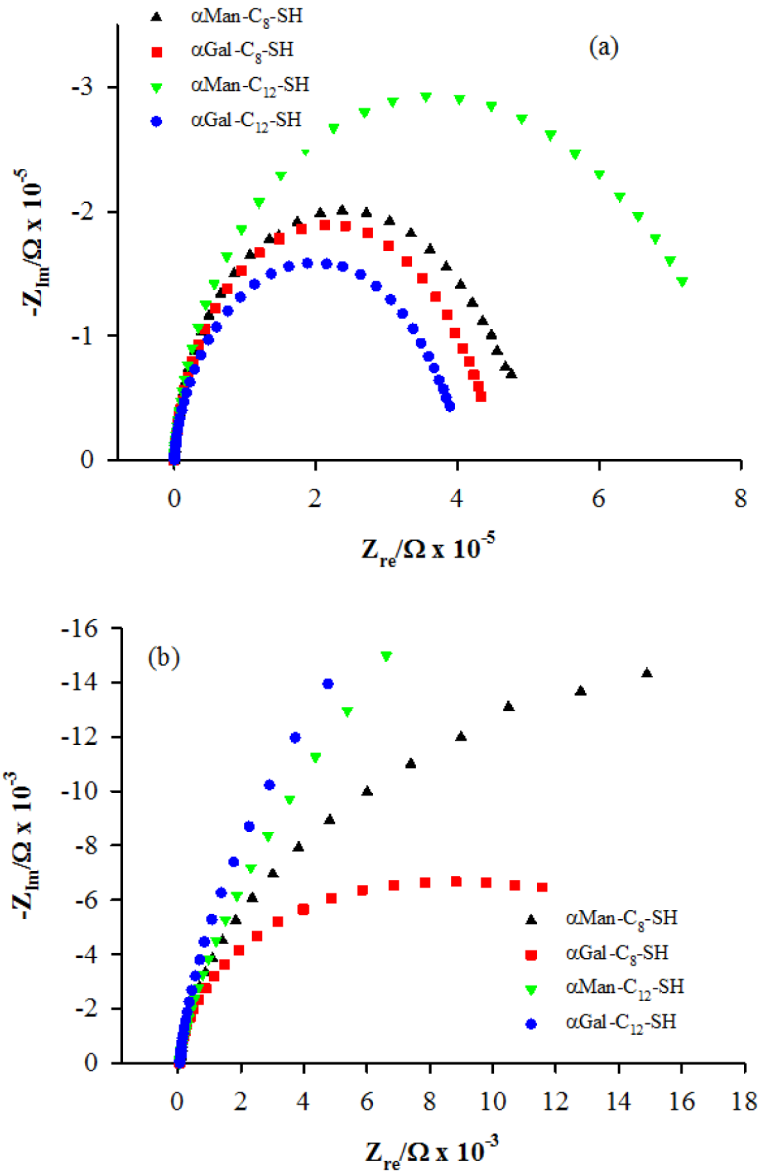

Fig. 5.

Nyquist plots for the carbohydrate-terminated (mannose or galactose) SAMs: αMan-C_8-SH (up triangles), αMan-C_{12}-SH (down triangles), αGal-C_8-SH (squares), and αGal-C_{12}-SH (circles) on (a) Au wire and (b) np-Au, in each case for one of the set of three independently prepared electrodes.

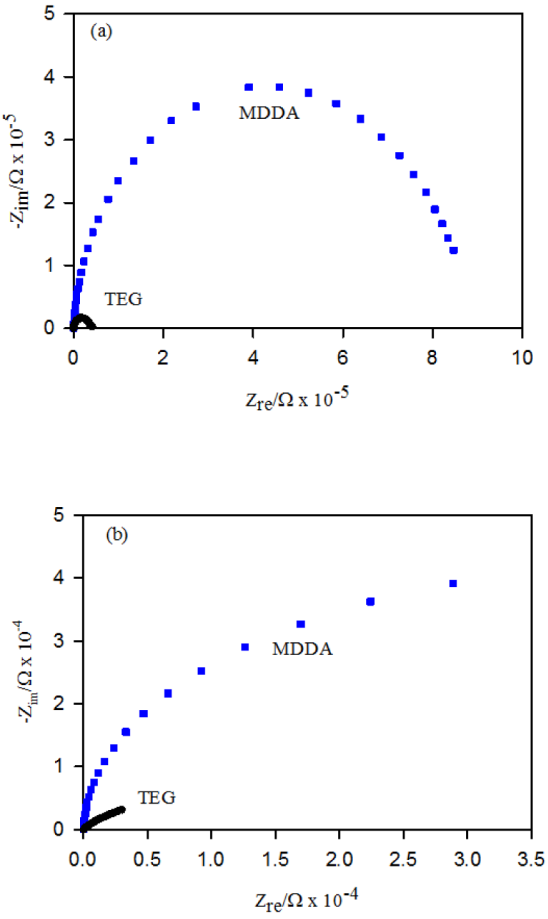

Fig. 6.

Nyquist plots for mercaptododecanoic acid (MDDA) and HO-PEG_2-SH SAMs on (a) Au wire and (b) np-Au, in each case for one of the set of three independently prepared electrodes.

Table I

The apparent electron transfer rate constants for gold wire electrodes and np-Au covered Au wire electrodes modified with alkanethiol SAMs. The data shown are for measurements on three independently prepared SAM modified electrodes.

SAM Molecule	Surface	R_{ct}(kΩ)	R_{ct}(kΩ cm^2)	k_{app} (cm s^{-1})	log (k_{app})
Octanethiol	Au	682 ± 168	21.8	2.23×10^{-6}	−5.65
	np-Au	255 ± 103	3264	1.49×10^{-8}	−7.82
Decanethiol	Au	1423 ± 110	45.5	1.07×10^{-6}	−5.97
	np-Au	1308 ± 323	16742	2.91×10^{-9}	−8.53
Dodecanethiol	Au	1881 ± 780	60.2	8.10×10^{-7}	−6.09
	np-Au	1798 ± 118	23014	2.12×10^{-9}	−8.67
Tetradecanethiol	Au	2707 ± 527	86.6	5.63×10^{-7}	−6.24
	np-Au	2760 ± 290	35328	1.38×10^{-9}	−8.86

Table II

The apparent electron transfer rate constants for gold wire electrodes and np-Au covered Au wire electrodes modified with mannose or galactose-terminated SAMs, with mercaptododecanoic acid, and with HO-PEG_2-SH. The data shown are for measurements on three independently prepared SAM modified electrodes.

SAM Molecule	Surface	R_{ct}(kΩ)	R_{ct}(kΩ cm^2)	k_{app} (cm s^{-1})	log (k_{app})
αMan-C_8-SH	Au	411 ± 84	13.2	3.69×10^{-6}	−5.43
	np-Au	15.3 ± 3.1	196	2.49×10^{-7}	−6.60
αMan-C_{12}-SH	Au	747 ± 175	23.9	2.04×10^{-6}	−5.69
	np-Au	17.4 ± 4.1	223	2.19×10^{-7}	−6.66
αGal-C_8-SH	Au	413 ± 77	13.2	3.69×10^{-6}	−5.43
	np-Au	11.2 ± 1.0	143	3.41×10^{-7}	−6.47
αGal-C_{12}-SH	Au	208 ± 47	6.66	7.32×10^{-6}	−5.14
	np-Au	21.1 ± 3.1	270	1.81×10^{-7}	−6.74
COOH-C_{12}-HS	Au	848 ± 29	27.1	1.80×10^{-6}	−5.74
	np-Au	86.9 ± 7.6	1112	4.39×10^{-8}	−7.36
HO-PEG_2-SH	Au	42 ± 15	1.34	3.64×10^{-5}	−4.44
	np-Au	0.14 ± 0.02	1.79	2.72×10^{-5}	−4.56